CRYSTAL GROWTH & DESIGN

Article

pubs.acs.org/crystal

Pitch-Induced Bandgap Tuning in Self-Catalyzed Growth of Patterned GaAsSb Axial and GaAs/GaAsSb Core−Shell Nanowires Using Molecular Beam Epitaxy

Manish Sharma,[†] Md Rezaul Karim,[†] Pavan Kasanaboina,[‡] Jia Li,[†,‡] and Shanthi Iyer*[,†,‡]

[†]Nanoengineering, Joint School of Nanoscience and Nanoengineering, North Carolina A&T State University, Greensboro, North Carolina 27401, United States

[‡]Department of Electrical and Computer Engineering, North Carolina A&T State University, Greensboro, North Carolina 27411, United States

ABSTRACT: We report on the pitch-induced bandgap tuning in GaAsSb (axial) and GaAs/GaAsSb (core−shell) patterned vertical nanowire (NW) arrays grown by Ga-assisted molecular beam epitaxy on Si(111). Red shifts in the range of 40−50 meV in the 4 K micro-photoluminescence (μ-PL) spectral peaks have been observed, for NW arrays with pitch length variation from 200 to 1200 nm, in the axial and core−shell configurations. The variation in the PL peak intensity closely follows the optical absorption dependency on the pitch length of the NW array computed using finite dimension time domain simulation. A semiempirical mass conservation of the growth-species-based-model has been proposed encompassing different material pathways. The secondary fluxes re-emitted from the side facets of the neighboring NWs contribute substantially toward the growth for smaller pitch lengths, while those from the oxide surface dominate at larger pitch lengths for high V/III beam equivalent pressure ratios. Excellent agreement between the experimental and simulated results have been observed for the pitch dependent axial and radial NW dimensions of both the axial and core−shell configured GaAsSb NWs. This study shows great promise for the applicability of patterned NWs for band gap tuning by simply varying the NW array pitch length.

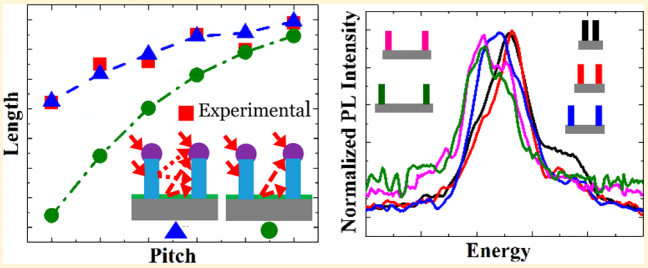

1. INTRODUCTION

Currently, nanowires (NWs) are extensively explored due to their one-dimensional architecture and high aspect ratio enabling better stress−strain management,[1,2] optical trapping,[3−5] and quantum confinements.[6,7] Commercialization of the NW-based electronic devices requires demonstration of scalability and reliable performance, which can be achieved by site-specific growth on prepatterned substrates. The well-defined patterned array of NWs enables independent tuning of the diameter and length. It also influences NW morphology due to variation in pitch-induced growth kinetics caused by the alteration in the availability of the growth species.[8,9] Initial reports of pitch dependent analytical modeling of the growth rate were based on a mass continuity model for patterned NWs, utilizing the contributions of the flux components of direct impingement and reflection from the oxide to the droplet. Since then, it has advanced to include the effects of pattern opening diameter and shadowing of the oxide-scattered fluxes by neighboring NWs, and more recently to delineating their contribution to both the axial and radial growth.[9−11]

Extensive work has been reported by Tomioka et al.[12] using the electron beam lithography (EBL) technique for patterned growth of III−V NWs using metal organic vapor phase epitaxy (MOVPE). However, patterned growth of III−V NWs using molecular beam epitaxy (MBE) requires stringent control of several growth parameters concurrently; therefore, their interdependencies pose a challenge.[13,14] In recent years, GaAsSb NWs have been a focus of interest as they encompass a short wavelength range essential for nanoscale sources and detectors in telecommunication applications, photonic integrated circuits, and quantum information science. Additionally, the presence of two group-V elements offers a distinct advantage in terms of better compositional homogeneity as opposed to other potential alternative material systems in this wavelength range, mainly InGaAs NWs.[15] Despite its potential, work on GaAsSb patterned arrays has been minimal[16,17] and is further limited to the axial configuration only. There has been no study of the mechanism of pitch-induced variation in growth rates of GaAsSb NWs, although it is well-established that the presence of Sb in growth environment changes the growth rate attributed to its surfactant effect.[18]

In this work, we present pitch-induced effects on the geometry and optical characteristics of patterned GaAsSb NWs, grown by self-assisted MBE, in both axial and core−shell (C−S) configurations. An existing analytical model by Gibson et al.[11] has been extended to incorporate the growth species desorbed from the NW side facets as an additional material supply pathway, due to the high V/III ratio used in our growth. The

Received: October 26, 2016
Revised: December 9, 2016
Published: December 22, 2016

DOI: 10.1021/acs.cgd.6b01577
Cryst. Growth Des. 2017, 17, 730−737

compliance of the devised model was corroborated initially on the GaAs NWs geometry and then extended to the case of GaAsSb axial and GaAs/GaAsSb C−S NWs. Pitch-induced composition modulation in the GaAsSb axial and GaAS/GaAsSb C−S NWs leading to a shift in the PL peak energies has been demonstrated for the first time.

2. EXPERIMENTAL DETAILS

The NWs were grown via a vapor−liquid−solid (VLS) mechanism in an EPI 930 solid source MBE system with valved As and Sb cracker sources. Self-assisted growth epitaxy was used with the initiation of the growth by an impingement of Ga flux, which serves as a catalyst, on the substrate prior to opening of As_4 flux. An As beam equivalent pressure (BEP) of 4.8×10^{-6} Torr was used and the GaAs stem of 200 nm for axial growth and ∼2−3 μm of GaAs core−shell for C−S growths were grown at a substrate temperature of 620 °C. GaAsSb growth in the axial configuration was initiated by opening the Sb flux at a BEP of 9.6×10^{-7} Torr with concurrent reduction of As_4 BEP to 3.8×10^{-6} Torr, the details of which are provided in Ahmad et al.[19] For the GaAs/GaAsSb C−S NWs, growth of the core was terminated by simultaneous shutting of both the Ga and As shutters, and the substrate temperature was lowered to 570 °C where both these sources were opened again along with the Sb source for the commencement of shell growth, the details of which are provided in Kasanaboina et al.[15]

Selected area growth of nanowires was achieved by patterning holes on Si(111)/SiO_2 (150 Å) using a combination of electron beam lithography (EBL) and reactive ion etching (RIE). Thermally oxidized Si wafers were spin coated with poly(methyl methacrylate) (PMMA) resist and patterns of (100 × 100) arrays of holes with varying pitch lengths of 200 to 1200 nm were then created using an ELS-7500EX electron beam tool. These were developed and dry etched using Trion Technology Phantom II reactive ion etcher. Any residual PMMA and native oxide from the patterned holes were subsequently removed using oxygen RIE and 2% HF solution, respectively.

Having the substrate preparation optimized for selective area growth, two other vital growth parameters, namely, Ga shutter opening time and V/III ratio, were optimized for pattern growth of GaAs NWs. For a given Ga shutter opening duration, the V/III ratio was varied to obtain hole occupancy >90% on the patterned surface. The growth and processing parameters, namely, RIE etching time, HF etching, Ga shutter opening time, and V/III ratio were optimized for GaAs NWs, which were then translated to the growth of GaAs/GaAsSb C−S and GaAsSb axial NWs.

The surface morphology and dimensions of the grown NWs were characterized by using a Carl Zeiss Auriga-BU FIB field emission scanning electron microscope (FESEM), with the X-ray energy dispersive spectroscopy (EDS) attachment being used to determine the composition of the NWs. Optical characteristics of the NWs were measured by μ-PL at 4K using a 633 nm He−Ne laser as the excitation source, the details of which are provided in Kasanaboina et al.[15]

3. GROWTH RATE MODELS

The growth species can reach the droplet at the NW tip and side-facets in numerous ways, namely, direct impingement from the primary molecular beam flux, adsorption of secondary/re-emitted fluxes (fluxes comprising atoms/molecules desorbed off and/or scattered from the substrate surface and NW facets), and adatom diffusion on the substrate and/or along the side facets.[8,10,11,20] Relative contributions toward axial and radial growth depend on various factors: (i) the effective beam area intercepted by droplets or facets,[11,21] (ii) shadowing of the direct impinging flux,[10] (iii) shadowing of the line-of-sight re-emitted flux[9] (which will be henceforth referred to as shading) by the neighboring NWs, and finally (iv) diffusion lengths of the growth species on the substrate and facets.[10,14,20,22] Surface diffusion on the SiO_2 surface is assumed to be negligible due to the short migration length of both the Ga and As adatoms prior to desorption from the surface.[11,23] In addition, the contributions of the group-V adatoms diffusing on the sidewalls are also neglected as the surfactant effect of Sb is expected to trim the diffusion lengths of group-V adatoms.[11,18]

However, secondary re-emitted fluxes contribute significantly[8,11] to the growth of NWs, which become readily perceivable when the NWs are grown in a predefined array.[24] The amount of secondary flux re-emitted is reported to be pitch dependent. For instance, with the decrease in the pitch length of the NW-array, secondary flux re-emitted from the oxide surface is attenuated,[9−11] while those from the side-facets are augmented.[24,25] Thus, individual contributions to the NW growth would have opposite impacts on the growth rates.[25] Therefore, simultaneous contributions of these two would lead to a more gradual variation in the growth rate with the pitch length, as observed in our ternary NWs. In the following, we describe the growth rate model encompassing the effect of re-emission from NW side-facets in the growth model reported by Gibson et al.[11]

In the case of self-catalyzed VLS growth of III−V nanowires, the droplet is continuously replenished by group-III atoms from either primary or secondary fluxes or by diffusion through the NW side-facets as discussed above. As a result, axial growth is considered to be limited by the availability of group-V atoms.[26] Simultaneous occurrence of NW growth along radial direction is commonly modeled as a vapor−solid growth mechanism, which is rate limited by the availability of group-III atoms.[11] We consider three possible pathways for both group-V and group-III species supplies to the droplet and side-facets: direct impingement from the molecular beam, adsorption of re-emitted fluxes from the oxide surface, and from the NW side-facets. For a cylindrical configuration of NW of length, L, and radius, R, the incremental change in length, dL, of the NW with respect to an equivalent planar deposition of thickness, dh, of the group-V species is given as

$$\frac{dL}{dh} = \Gamma_a\left(\frac{dL}{dh_p} + \frac{dL}{dh_{ss}} + \frac{dL}{dh_{sf}}\right) \quad (1)$$

The first two terms on the right side of eq 1 represent the contributions of the primary group-V beam and secondary group-V flux scattered from the oxide surface, respectively, as described by Gibson et al.,[11] while the third term accounts for the contribution of secondary group-V flux re-emitted from NW side-facets. It should be noted that group-V fluxes (both primary and secondary) refer to the combined fluxes of all the group-V species present in the growth environment. The incorporation factor, Γ_a, is the ratio of the amount of the species being consumed in the axial growth process to the total collected material by the droplet.[11] Similarly, the radial extension, dR, per equivalent planar deposition can be expressed as

$$\frac{dR}{dh} = \Gamma_r\left(\frac{dR}{dh_p} + \frac{dR}{dh_{ss}} + \frac{dR}{dh_{sf}}\right) \quad (2)$$

In eq 2, the terms on the right side represent the radial growth rates due to the primary flux and secondary flux reflected from the oxide surface and the side facets, respectively, and Γ_r represents the effective sidewall incorporation factor.

Contributions of Primary Molecular Beam. Effective molecular beam cross-section intercepting the droplet at the NW tip depends on the contact angle β of the droplet with the NW top surface and the beam incident angle (α) with the normal direction to the substrate.[21] The incident angle in our MBE system is approximately 33°, and we determined the contact

DOI: 10.1021/acs.cgd.6b01577
Cryst. Growth Des. 2017, 17, 730−737

angle to be 120°. Under these conditions, the contribution of the primary beam to the axial growth rate can be expressed as[21]

$$\frac{dL}{dh_p} = \frac{1}{\sin^2\beta} \tag{3}$$

Radial growth rate due to primary Ga-flux can be written as[11]

$$\frac{dR}{dh_p} = \frac{\sin\alpha}{\pi} \tag{4}$$

Contributions of Fluxes Re-emitted from the Oxide Surface. The total flux intercepted by the droplet from the secondary flux scattered from the oxide surface can be computed by carrying out two integrations first, of the contribution of every point on the oxide surface to the line of site scattered flux adsorbed by a point on the droplet and second, of adsorption of every point on the droplet surface. However, in order to include the effect of shading from the oxide surface, the region around the base of a nanowire is divided into disjoint concentric annular regions between the concentric circles of radius ρ_i and ρ_{i+1} ($i = 0$, 1, 2, ...), and the degree of shading S_{ρ_i} is calculated using the appropriate geometric calculation.[9] Finally, axial growth rate due to oxide-scattered flux was computed from eq 5.[11]

$$\frac{dL}{dh_{ss}} = \sum_{i=0}^{\infty} S_{\rho_i} \int_{\rho_i}^{\rho_{i+1}} d\rho \int_{L}^{Z} dz \int_{0}^{\pi/2} d\phi \left[\left(\frac{2\pi R \cos\delta}{\sin\beta} \right) \times \left(\frac{2z\rho^2 \cos\delta \cos\phi}{(\rho^2 + z^2)^2} - \frac{2\rho z^2 \sin\delta}{(\rho^2 + z^2)^2} \right) \left(\frac{1}{\pi R^2} \right) \right] \tag{5}$$

Here, $Z = L + r(1 - \cos\beta)/\sin\beta$ represents the distance of a point on the droplet from the substrate, ϕ is the azimuth angle, and δ is the angle between the normal vectors of the substrate and the droplet.

Similarly, the radial growth rate due to the oxide-scattered secondary Ga-flux is expressed as[11]

$$\frac{dR}{dh_{ss}} = \sum_{i=0}^{\infty} S_{\rho_i} \int_{\rho_i}^{\rho_{i+1}} d\rho \int_{0}^{L} dz \int_{0}^{\pi/2} d\phi \left[(2\mu R) \times (2z\rho^2 \cos\phi) \times \left(\frac{1}{2\pi R L} \right) \right] \tag{6}$$

Contributions of Fluxes Re-emitted from the NW Facets. Incidence of reemitted secondary fluxes from the side facet on the droplet and side facets of neighboring NWs are schematically shown in Figure 1a,b, respectively. Group-V atoms incident on the side-facet of a NW either contribute to radial growth or desorb off to the growth environment, forming the side-facet scattered secondary flux.[11] We assume that re-emission of group-V atoms from NW side-facet is omnidirectional and secondary fluxes travel ballistically.[24] Further, we assume that re-emitted flux from only the nearest half-surface of a NW can reach the droplet or side-facet of a neighboring NW. Then the volume, dV, of group-V materials reaching the droplet or side-facets of a NW from side-facets of the neighboring NW at any instant can be approximated as

$$dV = \pi R L \, dR \times \Psi \tag{7}$$

Here, dR is the thickness of the group-V layer being desorbed and Ψ is the readsorption probability defined as the ratio of the solid angle created by the adsorbing surface and solid angle of all possible re-emission directions. For the droplet at NW tip, the readsorption probability is computed from[24]

$$\Psi_d = \frac{R^2}{pL} \tan^{-1}\left(\frac{L}{p}\right) \tag{8}$$

where p is the pitch length of the array. Therefore, the contribution of the side-facet scattered secondary group-V flux to the axial growth rate may be calculated as

$$\frac{dL}{dh_{sf}} = \chi_p \frac{R}{p} \tan^{-1}\left(\frac{L}{p}\right) dR_V \tag{9}$$

Here, the factor χ_p is a lumped parameter that considers the effective number of NWs from which the side-facet scattered secondary fluxes reach the central NW and desorption probability of the side facets.

Following a similar approach mentioned by Li et al.,[24] the readsorption probability for the side-facet of a NW from an adjacent NW side-facet was calculated to be

$$\Psi_f = \frac{2R}{\pi p} \tan^{-1}\left(\frac{L}{2p}\right) \tag{10}$$

The radial growth rate due to side-facet scattered secondary Ga-flux may thus be calculated as

$$\frac{dR}{dh_{sf}} = \chi_p \frac{R}{\pi p} \tan^{-1}\left(\frac{L}{2p}\right) dR_{III} \tag{11}$$

$dR_{V/III}$ in eq 9 and eq 11 are the estimated change in radial direction due to an impingement of corresponding growth species on the side-facets (see Figure 1c for a comparison of dR_V and dR_{III}).

Shell Growth Rate. Although the Ga flux intercepted by the droplet at NW tip is not likely to contribute to the radial growth, in the absence of the droplet, Ga atoms incident on the NW-top surface might diffuse to the side facets, providing an auxiliary amount of group-III material for enhanced lateral growth of the NW. Therefore, we consider this additional pathway of Ga adatom supply to the side-facets and express the shell thickness growth rate as follows:

$$\frac{dT}{dh} = \Gamma_t \left(\frac{dT}{dh_p} + \frac{dT}{dh_{ss}} + \frac{dT}{dh_{sf}} + \frac{dT}{dh_{top}} \right) \tag{12}$$

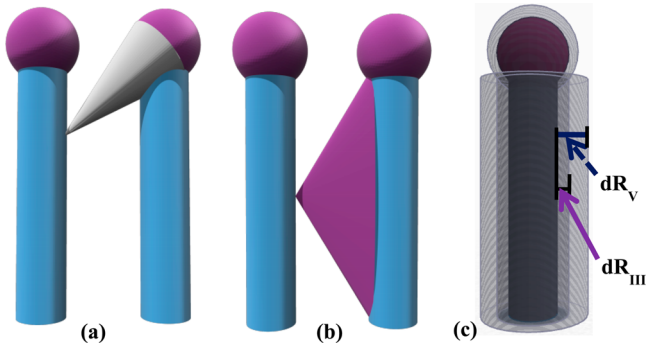

Figure 1. Illustration of the side facet re-emitted flux impinging on (a) the droplet, (b) the side facet of nearby NWs, and (c) hypothetical group-III and group-V layers formed by species adsorbed on side facets used for the calculation of the radial increment.

DOI: 10.1021/acs.cgd.6b01577
Cryst. Growth Des. 2017, 17, 730−737

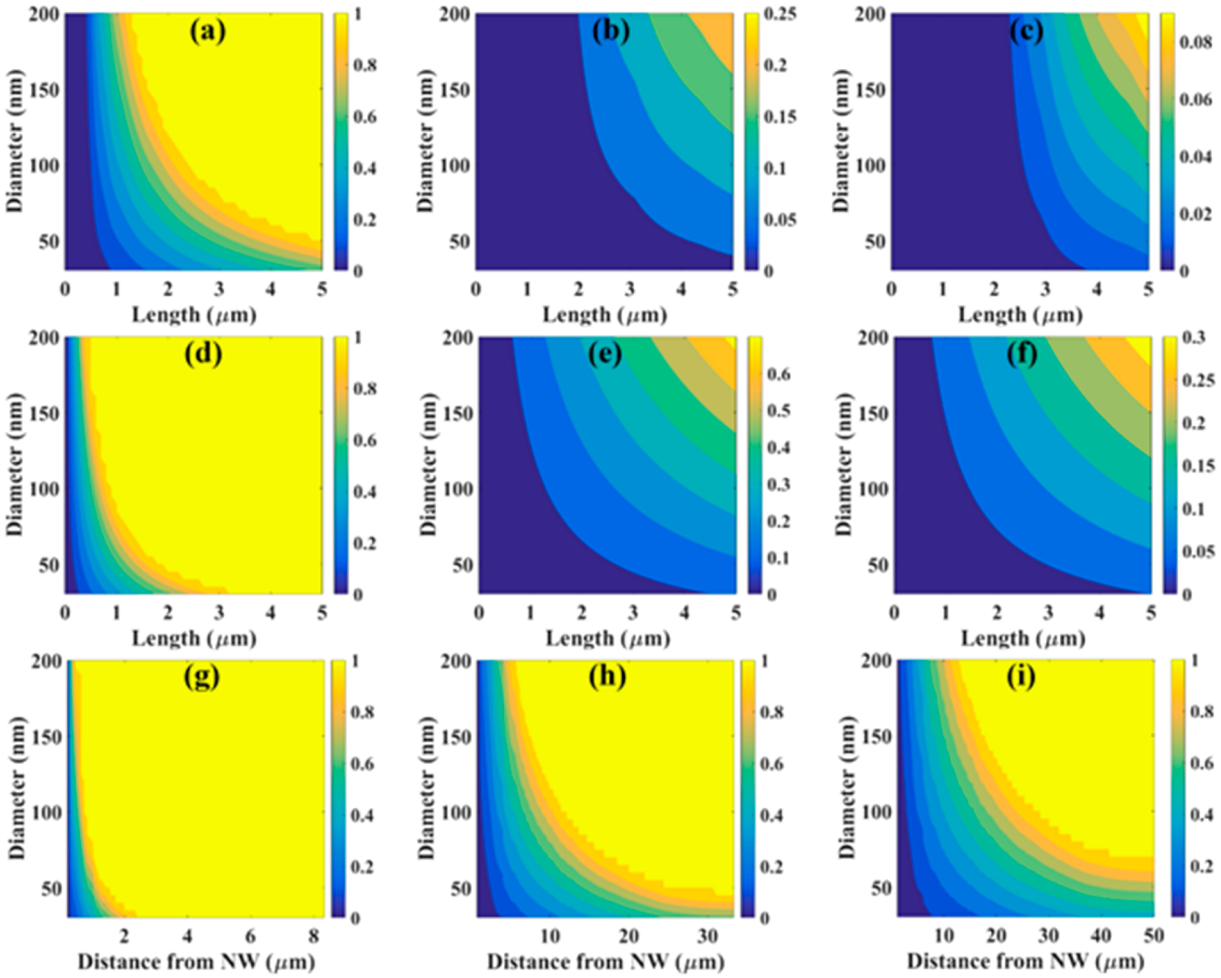

Figure 2. Percentage reductions in adatoms: (a–c) impinging on side-facets, (d–f) on the oxide surface due to shadowing of primary molecular beam flux, and (g–i) due to shading of secondary flux reemitted from the oxide surface as functions of the diameter of surrounding NWs and distance from the center NW under investigation. Shadowing and shading were calculated for the pitch lengths of (a, d, g) 200 nm, (b, e, h) 800 nm, and (c, f, i) 1200 nm.

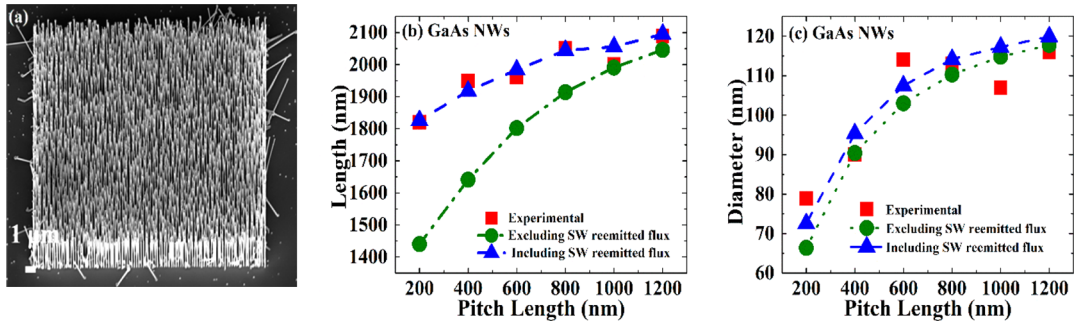

Figure 3. SEM micrograph of a typical patterned GaAs NW array for a pitch length of 200 nm (a). Pitch dependency of GaAs NWs: (b) lengths, and (c) diameters calculated without (green circles) and with (blue triangles) considering the side-wall (SW) re-emitted flux compared to the experimental results (red squares), which are the averages of the lengths and diameters of 25 NWs with standard deviations of ∼30 nm and ∼4.5 nm, respectively.

Here, $\frac{dT}{dh_{top}}$ is the contribution of the new pathway, which should scale with the ratio of NW top-surface area to the side-facet area (i.e., $\pi R^2/2\pi RL$). The remaining terms are similar to those in the radial growth rate equation.

Reduction in Fluxes. The amount of growth species collected by the droplet as well as the side facets are reduced by shadowing of the primary beam and shading of re-emitted fluxes by the neighboring NWs in the array. The shadowing affects the side-facet collection, whereas the shading affects both the droplet and the side-facet collections of growth species.[9,10] With decreasing pitch length, the shadowing effects become significant. Therefore, modeling of the growth of NW array necessitates appropriate quantification of the contributions from shadowing and shading of the respective primary and secondary fluxes. We calculate the effects of shadowing of the primary flux following Madsen et al.[10] and shading of re-emitted secondary fluxes from the oxide layer following Kelrich et al.[9] The shadowing effect is influenced by the length and diameter of the NWs in the array, while shading depends on the diameter of

DOI: 10.1021/acs.cgd.6b01577
Cryst. Growth Des. 2017, 17, 730–737

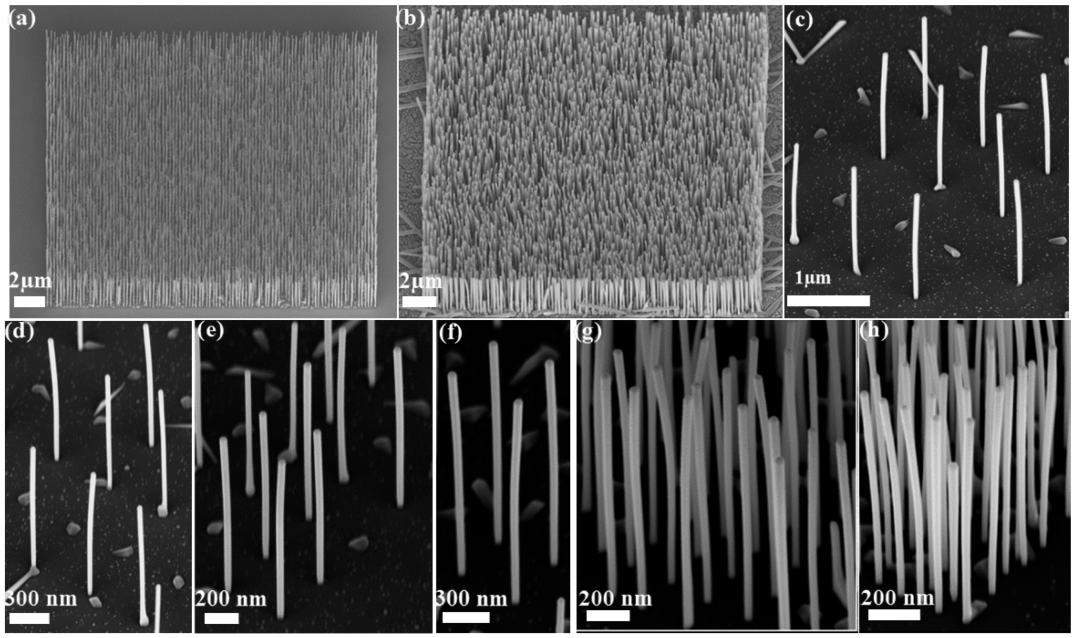

Figure 4. SEM images of (a) GaAsSb axial and (b) GaAs/GaAsSb core−shell NW arrays for a pitch length of 200 nm. (c−h) High magnification SEM images of self-catalyzed GaAsSb NWs grown on Si(111) substrate covered by SiO_2 layer with holes of 80 nm average diameter for different pitch lengths of 1200, 1000, 800, 600, 400, and 200 nm.

surrounding NWs and lateral distance from the NW on the substrate. The percentage reductions in collected growth species on the droplet and side-facet due to shadowing and shading in NW arrays with pitch lengths of 200, 800, and 1200 nm are depicted in Figure 2. Demonstrably, the primary flux incident on both the NW side facets and the oxide surface is severely suppressed by shadowing for the lowest pitch length, while only by 10% and 30%, respectively, for the largest pitch length. Similarly, shading of oxide re-emitted flux significantly shrinks the secondary flux collection region for the lower pitch lengths. Additionally, effects of shadowing and shading are enhanced with increasing length and diameter of the neighboring NWs.

4. RESULTS AND DISCUSSION

Growth Rates of GaAs Nanowires. Figure 3a shows representative GaAs NW array of 200 nm pitch length grown under optimized conditions. All the NWs reported in this paper are predominantly zinc-blende in crystal structure. In order to ascertain the contribution of side facet re-emitted flux to the growth of NWs, a comparison of the length and diameter of GaAs NWs computed using eq 1 and eq 2, respectively, made, considering both the presence and absence of side facet re-emission. The average diameter of the pattern openings on the oxide surface was measured to be 80 nm, while the initial droplet radius was estimated to be 28 nm, corresponding to 10 s Ga predeposition time, regardless of the array's pitch lengths. This is consistent with the results of Plissard et al.[13] For the V/III BEP ratio of 20 used in this study, an equivalent planar deposition rate of Ga of 0.2 nm/s[27] along with measurements of $\beta = 120°$ and $\alpha = 33°$ were used in all calculations. The set $\{\chi_p\}$ was extracted from the best simulated fit of the lengths and diameters of GaAs NWs to the corresponding experimental data for different pitch lengths. The shadowing and shading illustrated in Figure 2 are simulated for vertical NWs with no parasitic growth between the NWs and thus were adjusted to mimic the actual growth.

As is evident from Figure 3b,c, which displays the calculated and measured lengths and diameters of GaAs NWs, respectively, pitch length plays an important role in material collection. Excellent agreement with our experimental data is obtained with the inclusion of side-facet re-emitted secondary flux. The latter significantly affects the axial growth rate for smaller pitch dimension and also diminishes the large variations in the axial growth rates with pitch length. As the V/III BEP ratio (=20) used in this study is significantly higher than the published reports of the V/III flux ratio of 1.8 used by Gibson et al.,[11] the number of As atoms incident on the side-facets is expected to exceed those consumed in the radial growth. In addition, the excess As atoms are expected to get desorbed off from the side-facets due to the low diffusion length of As, with only a fraction of this flux reaching the droplets and side-facets of adjacent NWs. Therefore, lower pitch dimensions corresponding to higher density NWs result in an increased contribution of scattered As from the side facets, which is likely responsible for the enhanced growth rate observed in our study. The continual reduction in the contribution of scattered As from the side-facets with increasing pitch length ultimately causes the primary flux, and the re-emitted flux from the oxide surface to be the main contributor to the growth rate. This explains the smaller variation observed in the growth rates with increasing pitch length as expected.[24,25] In contrast, contribution of the scattered As from the side facets is found to have only a minimal effect on the diameter of the NWs and hence the radial growth rates (Figure 3c). This is attributed to the vapor−solid mechanism being responsible for the radial growth where the growth is limited by the availability of Ga. Therefore, the effect of Ga scattered from the side facet is less marked, despite the high As to Ga BEP ratio used in our work.

The best fit of the simulated data to the experimental values of NW dimensions was found for axial and radial incorporation factors Γ_a and Γ_r of ∼0.83 and ∼0.37, respectively, and findings indicate that 83% of the group-V species adsorbed on the droplet and 37% of the group-III species adsorbed on the side facets contributed to the respective growths. As discussed earlier, the remaining collected species are lost in the growth environment due to desorption from the droplet and the diffusion toward the

DOI: 10.1021/acs.cgd.6b01577
Cryst. Growth Des. 2017, 17, 730−737

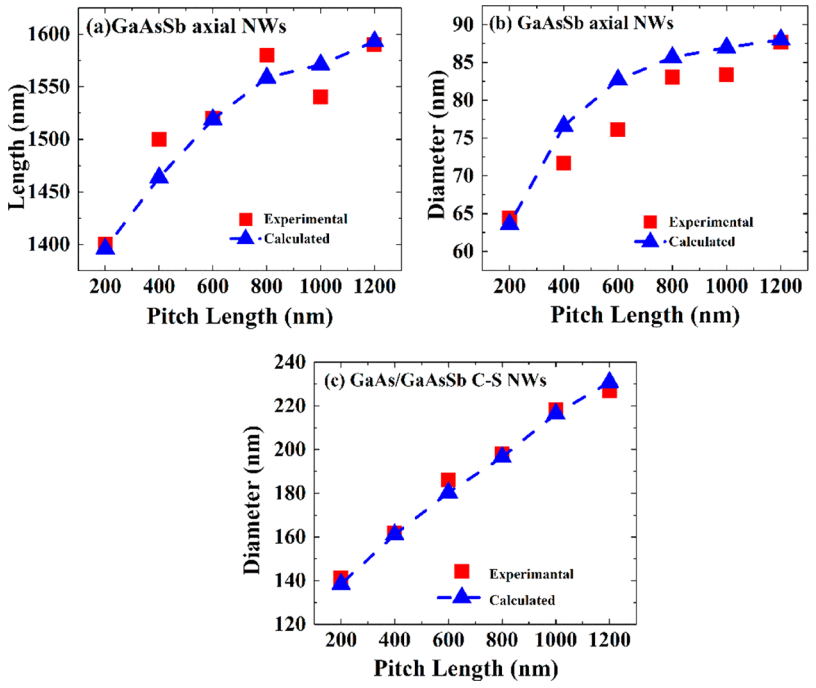

Figure 5. Superimposition of computed data on the experimental pitch length dependency of (a) lengths and (b) diameters of GaAsSb axial NWs, and (c) diameters of GaAs/GaAsSb C−S NWs. Experimental data represents the average values measured over 25 NWs with standard deviations in the lengths and diameters of the axial NWs being ∼30 nm and ∼3 nm, respectively, and diameters of the C−S NWs ∼5 nm.

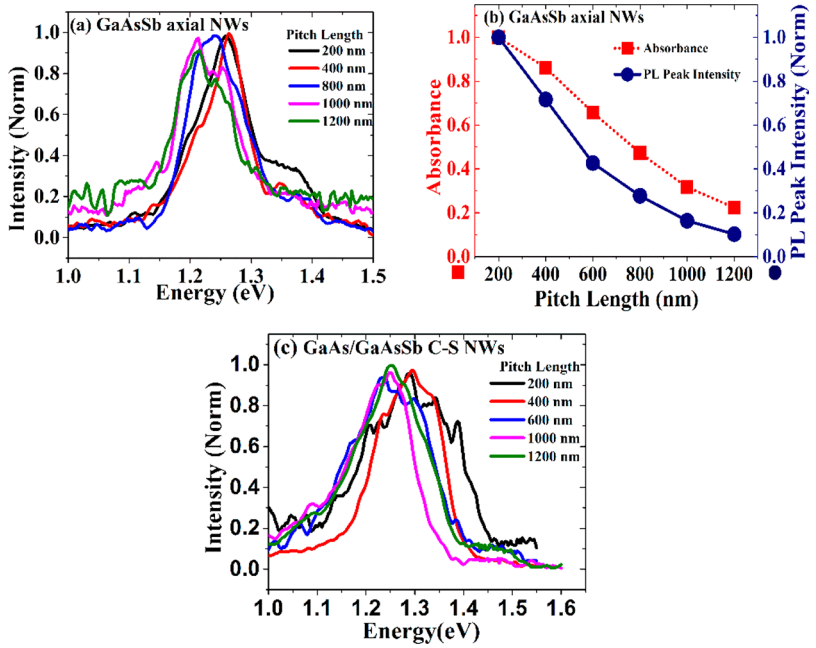

Figure 6. Pitch length dependency of (a) the PL spectra for GaAsSb axial NWs, (b) normalized PL intensity and absorbance @ 630 nm for GaAsSb axial NWs, and (c) PL spectra for GaAs/GaAsSb C−S NWs.

droplet along or desorption from the side facets. These axial and radial incorporation factors are in good agreement with those reported by Gibson et al.[11]

Growth Rates of GaAsSb Axial and GaAs/GaAsSb Core−Shell NWs. Figure 4a,b displays SEM images of GaAsSb axial and GaAs/GaAsSb C−S array NWs, respectively, for a pitch length of 200 nm. Figure 4c−h demonstrates the high magnification SEM images of partial axial GaAsSb NW arrays in descending order of pitch lengths from 1200 to 200 nm. Plots of the lengths and diameters of the nanowires in Figure 5a,b with pitch length show increase from 1.4 to 1.59 μm and 64−88 nm, respectively, with pitch lengths varying from 200 to 1200 nm. The diameters of the NWs are smaller than GaAs NWs due to the use of lower Ga predeposition time of 8 s time used for these growths, leading to a comparatively lower initial radius, estimated to be ∼23 nm. The lengths and diameters of GaAsSb axial nanowires have been calculated using approximately the same set $\{\chi_p\}$ quantified for GaAs NWs and compared to the experimental data, as presented in Figure 5, panels a and b, respectively. Reasonable agreement between the two further attest to the

DOI: 10.1021/acs.cgd.6b01577
Cryst. Growth Des. 2017, 17, 730−737

accuracy of the proposed model. The values of the incorporation factors Γ_a and Γ_r those resulted in the best fit to the experimental data were approximately 0.64 and 0.41, respectively. The value of Γ_a is significantly reduced as compared to the GaAs NWs.

The different values of Γ_a and Γ_r do not necessarily indicate the altered gross material collection on the droplet and the side facets; rather, it implies that the actual amount of growth species being consumed in the growth process has been altered. Several factors might account for the observed alterations in the values of Γ_a and Γ_r. First, let us focus on the reduction of axial incorporation factor. Sb-segregation results in a floating layer on the droplet surface,[18] which may reduce the effective amount of group-V species collected by the Ga-droplet and consequently lower the value of Γ_a. The three factors that favor the Sb-segregation have been identified to be smaller surface energy, larger atomic size of Sb than As and As−Sb intermixing and phase separation.[18] The addition of Sb leads to lowering the surface energy at the vapor−droplet and droplet−solid interface, which changes the contact angle due to droplet expansion.[16]

Thus, wetting angle-induced change in nucleation and growth-mode[16,25] is likely responsible for the observed effective amount of group-V species collected by the Ga droplet. In contrast, there is only a marginal increase in the value of Γ_r from GaAs NWs. Sb inhibits the adatom mobility[18] and thus mitigates the loss of Ga from the side facets by impeding the migration of Ga adatoms toward the droplet. Also, as the surface diffusion of Sb is much higher than As,[17] it indicates that more binding of Ga is likely to occur on the facets of GaAsSb axial NWs than GaAs NWs. Therefore, the percentage of Ga consumed in the radial growth process is higher in GaAsSb axial NWs over GaAs NWs, which explains the increase in Γ_r. Figure 5 illustrates both the experimental and computed (using eq 12) diameters of the GaAs/GaAsSb C−S NWs as a function of pitch length. Although solidification of the Ga droplet after the growth of the core suppresses any axial growth during the shell growth,[15] we observed occurrence of small axial growth that might be a result of incomplete solidification of the droplet as well as continuation of vapor−solid growth process at the NW tip. Hence, a constant diffusion from the NW top surface has been included. However, this contribution depends on the pitch length of the array since diameter to the length ratios of the NWs varies with it. Moreover, the diminished axial growth rate results in an increased availability of the group-V species for binding with Ga adatoms, which explains a much larger value of Γ_t (∼0.65) as compared to Γ_r in GaAsSb and GaAs NWs, as well as the linear variation of the diameter with pitch length.

4K μ-PL spectra of these ternary NWs in Figure 6a,c reveal that with an increase in pitch length, the PL peak energy exhibits a redshift of approximately 45 meV in the GaAsSb axial and approximately 40 meV in the GaAs/GaAsSb C−S NWs array. Sb composition, as determined from EDS, was found to increase from 4 to 7 atom % in the GaAsSb axial and 3.5 to 6 atom % in the GaAs/GaAsSb C−S configuration. It is to be noted that EDS attached to SEM is commonly known to underestimate the Sb composition. We surmise that the desorption rates of As and Sb from the oxide surface and the NW side facets are different and as evinced by our growth rate model, increases in pitch length of the array enhance the collection of the oxide re-emitted group-V flux, while reduce the collection of the latter, introducing variation in composition, leading to the observed shifts in the PL peak energies. The presence of multiple peaks is attributed to the presence of defects, particularly at the base segment of the NWs and compositional inhomogeneity in NWs,[28] which broadens the full width half maxima (fwhm). The growth conditions used in this work have not been optimized to obtain good quality NWs, but merely to attain vertical NWs with high yield. A finite difference time domain (FDTD) simulation of optical absorption in GaAsSb NWs, carried out at 630 nm illumination source wavelength, shows an excellent agreement with the PL peak intensity variation with the pitch length. Reduction in the substrate coverage for the larger pitch length results in reduction in the absorption of photons from fixed incident beam cross-section, hence reduces the emission intensity. The PL peak position and fwhm for higher pitch length in both axial and C−S configurations approach the same values obtained in conventional growth.

A good agreement between the values of incorporation factors for GaAs NWs obtained in this work and by Gibson et al.,[11] despite the use of widely different V/III flux ratios and different substrate temperatures, indicates the powerful nature of this modeling tool. It provides better insight into the various competing pathways that contribute to the collection of the materials. Further, distinct values of incorporation factors obtained in GaAsSb as compared to GaAs suggest that the model shows great promise for estimating the chemical composition of the NWs as well. Finally, the observed pitch-induced red shift in PL peak energies provides another pathway for bandgap tuning above and beyond the commonly used techniques of variation with growth temperature and BEP ratios of As to Sb.

5. CONCLUSION

This simple growth model for patterned NWs provides a better understanding of the growth environment. The secondary fluxes re-emitted from the side-facets are found to moderate the contrast in pitch-induced growth rates by the flux re-evaporated from the oxide layer on the substrate surface. Good agreement between the experimental and simulated NW dimensions of self-catalyzed GaAs, GaAsSb, and GaAs/GaAsSb C−S NWs attests to the efficacy of the proposed model. Furthermore, the values of incorporation parameters can be used as a tool for the comparison of incorporated species and the composition thereof. Finally, we have for the first time demonstrated pitch-induced band gap tuning in GaAsSb axial and C−S configurations, potentially providing a new pathway for band gap engineering. A combination of growth and optical modeling may prove to be a powerful tool toward designing ternary patterned NW array for a targeted wavelength.

AUTHOR INFORMATION

Corresponding Author

*E-mail: iyer@ncat.edu.

ORCID

Md Rezaul Karim: 0000-0002-1313-7095

Shanthi Iyer: 0000-0002-8163-9943

Notes

The authors declare no competing financial interest.

ACKNOWLEDGMENTS

This work is financially supported by Army Research Office (Grant No. W911NF-15-1-0160) and National Science Foundation (Award No. 1649517).

REFERENCES

(1) Johansson, J.; Dick, K. A. *CrystEngComm* **2011**, *13*, 7175−7184.

DOI: 10.1021/acs.cgd.6b01577
Cryst. Growth Des. 2017, 17, 730−737

(2) Cirlin, G. E.; Dubrovskii, V. G.; Soshnikov, I. P.; Sibirev, N. V.; Samsonenko, Yu. B.; Bouravleuv, A. D.; Harmand, J. C.; Glas, F. *Phys. Status Solidi RRL* **2009**, *3*, 112−114.
(3) Garnett, E. C.; Brongersma, M. L.; Cui, Y.; McGehee, M. D. *Annu. Rev. Mater. Res.* **2011**, *41*, 269−95.
(4) Garnett, E.; Yang, P. *Nano Lett.* **2010**, *10*, 1082−1087.
(5) Wallentin, J.; Anttu, N.; Asoli, D.; Huffman, M.; Åberg, I.; Magnusson, M. H.; Siefer, G.; Fuss-Kailuweit, P. F.; Dimroth, F.; Witzigmann, B.; Xu, H. Q.; Samuelson, L.; Deppert, K.; Borgström, M. T. *Science* **2013**, *339*, 1057−1060.
(6) Zhao, X.; Wei, C. M.; Yang, L.; Chou, M. Y. *Phys. Rev. Lett.* **2004**, *92*, 236805.
(7) Oncel, N.; van Houselt, A.; Huijben, J.; Hallback, A.-S.; Gurlu, O.; Zandvliet, H. J. W.; Poelsema, B. *Phys. Rev. Lett.* **2005**, *95*, 116801.
(8) Dalacu, D.; Kam, A.; Austing, D. G.; Wu, X.; Lapointe, J.; Aers, G. C.; Poole, P. J. *Nanotechnology* **2009**, *20*, 395602.
(9) Kelrich, A.; Calahorra, Y.; Greenberg, Y.; Gavrilov, A.; Cohen, S.; Ritter, D. *Nanotechnology* **2013**, *24*, 475302.
(10) Gibson, S. J.; LaPierre, R. R. *Nanotechnology* **2014**, *25*, 415304.
(11) Madsen, M. H.; Krogstrup, P.; Johnson, E.; Venkatesan, S.; Muhlbauer, E.; Scheu, C.; Sorensen, C. B.; Nygard, J. *J. Cryst. Growth* **2013**, *364*, 16−22.
(12) Tomioka, K.; Ikejiri, K.; Tanaka, T.; Motohisa, J.; Hara, J. M. S.; Hiruma, K.; Fukui, T. *J. Mater. Res.* **2011**, *26*, 2127−2141.
(13) Plissard, S.; Larrieu, G.; Wallart, X.; Caroff, P. *Nanotechnology* **2011**, *22*, 275602.
(14) Bauer, B.; Rudolph, A.; Soda, M.; Morral, A. F. i; Zweck, J.; Schuh, D.; Reiger, E. *Nanotechnology* **2010**, *21*, 435601.
(15) Kasanaboina, P. K.; Ojha, S. K.; Sami, S. U.; Reynolds, C. L., Jr.; Liu, Y.; Iyer, S. *Semicond. Sci. Technol.* **2015**, *30*, 105036.
(16) Conesa-Boj, S. C.; Kriegner, D.; Han, X. L.; Plissard, S.; Wallart, X.; Stangl, J.; Morral, A. F. i.; Caroff, P. *Nano Lett.* **2014**, *14*, 326−332.
(17) Ren, D.; Dheeraj, D. L.; Jin, C.; Nilsen, J. S.; Huh, J.; Reinertsen, J. F.; Munshi, A. M.; Gustafsson, A.; van Helvoort, A. T. J. V.; Fimland, B. O.; Weman, H. *Nano Lett.* **2016**, *16*, 1201−1209.
(18) Anyebe, E. A.; Rajpalke, M. K.; Veal, T. D.; Jin, C. J.; Wang, Z. M.; Zhuang, Q. D. *Nano Res.* **2015**, *8*, 1309−1319.
(19) Ahmad, E.; Ojha, S. K.; Kasanaboina, P.; Reynolds, C. L.; Liu, Y.; Iyer, S. *Semicond. Sci. Technol.*, in press.
(20) Glas, F.; Ramdani, M. R.; Patriarche, G.; Harmand, J. C. *Phys. Rev. B: Condens. Matter Mater. Phys.* **2013**, *88*, 195304.
(21) Glas, F. *Phys. Status Solidi B* **2010**, *247*, 254−258.
(22) Krogstrup, P.; Popovitz-Biro, R.; Johnson, E.; Madsen, M. H.; Nygard, J.; Shtrikman, H. *Nano Lett.* **2010**, *10*, 4475−4482.
(23) Giang, L. T. T.; Bougerol, C.; Mariette, H.; Songmuang, R. *J. Cryst. Growth* **2013**, *364*, 118−122.
(24) Li, A.; Sibirev, N. V.; Ercolani, D.; Dubrovskii, V. G.; Sorba, L. *Cryst. Growth Des.* **2013**, *13*, 878−882.
(25) Ramdani, M. R.; Harmand, J. C.; Glas, F.; Patriarche, G.; Travers, L. *Cryst. Growth Des.* **2013**, *13*, 91−96.
(26) Rieger, T.; Heiderich, S.; Lenk, S.; Lepsa, M. I.; Grutzmacher, D. *J. Cryst. Growth* **2012**, *353*, 39−46.
(27) Kasanaboina, P. K.; Ojha, S. K.; Sami, S. U.; Liu, Y.; Reynolds, C. L.; Iyer, S. *J. Electron. Matter* **2016**, *34*, 02L114.
(28) Farrell, A. C.; Lee, W. J.; Senanayake, P.; Haddad, M. A.; Prikhodko, S. V.; Huffaker, D. L. *Nano Lett.* **2015**, *15*, 6614−6619.

DOI: 10.1021/acs.cgd.6b01577
Cryst. Growth Des. 2017, 17, 730−737